All-Region DC Model for MOSFET with Physics-Based Parameter Extraction

Peter A. Sayegh* and Christopher Y. Ho† Columbia University, New York, NY
ELEN E6302 - Fall 2025

***Abstract*—This letter presents a physics-based approach for extracting device parameters and developing an all-region DC model for MOS transistors with uniform substrate. A systematic parameter extraction methodology is employed, utilizing transconductance-based threshold voltage extraction, geometry correction via $g_{m,max}$ extrapolation, and mobility degradation characterization. The model incorporates effective mobility dependence, body effect, and accounts for short-geometry effects.**

***Index Terms*—MOSFET modeling, parameter extraction, all-region model, effective mobility, threshold voltage.**

I. Introduction

ACCURATE compact models for MOS transistors are essential for circuit simulation and design. While sophisticated models exist in commercial simulators, understanding the physics-based parameter extraction process provides valuable insights into device behavior. This work develops a single-piece, all-region DC model following the methodology of Tsividis [1], with emphasis on systematic parameter extraction without trial-and-error approaches. All model parameters are extracted using physics-based criteria from measured I_D-V_{GS} and I_D-V_{DS} characteristics.

II. Parameter Extraction Methodology

A. Model

The model used here is a simplified body referenced all region model (PSP like), this means that it will be a surface potential-based model, and since this is a simplified model, the bulk charge across the channel is assumed linear and a mid-point surface potential is calculated as the average of the two potentials.

$$I_{DS1} = \frac{W}{L}\mu_{eff}C'_{ox}(V_{GB}-V_{FB}-\psi_{sm}-\gamma\sqrt{\psi_{sm}})(\psi_{s0}-\psi_{sL})$$

$$I_{DS2} = \frac{W}{L}\mu_{eff}C'_{ox}\alpha_m\phi_t(\psi_{s0}-\psi_{sL})$$

$$\alpha_m = 1+\frac{\gamma}{2\sqrt{\psi_{sm}}}$$

The surface potentials at the source (ψ_{s0}) and drain (ψ_{sL}) ends of the channel are obtained by iteratively solving the implicit equations:

$$\psi_{s0} = V_{GB} - V_{FB} - \gamma\sqrt{\psi_{s0}+\phi_t e^{(\psi_{s0}-2\phi_F-V_{SB})/\phi_t}} \quad (1)$$

*Email: pas2232@columbia.edu
†Email: cyh2119@columbia.edu

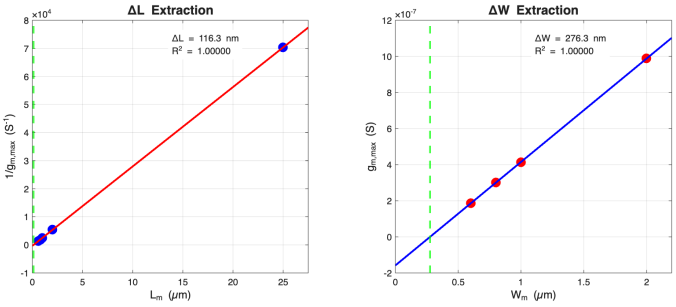

Fig. 1. ΔL And ΔW Extraction

$$\psi_{sL} = V_{GB} - V_{FB} - \gamma\sqrt{\psi_{sL}+\phi_t e^{(\psi_{sL}-2\phi_F-V_{DB})/\phi_t}} \quad (2)$$

B. Geometry Correction (ΔL and ΔW)

Effective channel dimensions differ from mask values due to lateral diffusion and other fabrication effects. Rather than assuming $\Delta L = \Delta W = 0$, we extract these parameters using transconductance measurements across multiple device geometries.

The peak transconductance scales as:

$$g_{m,max} \propto \frac{W_{eff}}{L_{eff}} = \frac{W_m - \Delta W}{L_m - \Delta L} \quad (3)$$

For devices with varying L (constant W), a plot of $1/g_{m,max}$ versus L_m yields ΔL from the x-intercept. Similarly, for varying W (constant L), $g_{m,max}$ versus W_m gives ΔW. This approach requires no model parameters, only measured transconductance data as can be seen in Fig. 1.

Results: Using devices with $L = 0.6$–25 μm and $W = 0.6$–25 μm at $V_{DS} = 0.1$ V:

$$\Delta L = 116.3 \text{ nm}, \quad \Delta W = 276.3 \text{ nm} \quad (4)$$

Both extractions achieved $R^2 > 0.9999$, indicating excellent linear fits.

C. Threshold Voltage and Body Effect

Threshold voltage V_T is extracted using the transconductance peak method. The peak of $g_m = dI_D/dV_{GS}$ marks the transition to strong inversion. To avoid weak/moderate inversion, the linear region ($V_{DS} = 0.1$ V) characteristic is fitted starting at $V_T + 4\phi_t$ (approximately 100 mV above the g_m peak).

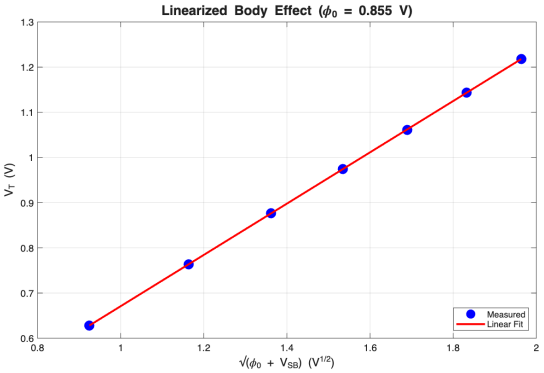

Fig. 2. ϕ_0, γ and V_{FB} extraction where N_A is given through the body effect coeffcient γ

The body effect is modeled as:

$$V_T(V_{SB}) = V_{FB} + \phi_0 + \gamma\sqrt{\phi_0 + V_{SB}} \tag{5}$$

where $\phi_0 = 2\phi_F + \Delta\phi$ accounts for surface potential and the transition region, and $\gamma = \sqrt{2qN_A\epsilon_{si}}/C_{ox}$ is the body effect coefficient.

Results: For $W_{eff} = 24.72$ μm, $L_{eff} = 0.884$ μm device:

$$\begin{aligned} \phi_0 &= 0.8553V \\ V_{T0} &= 0.6282 \text{ V} \quad (V_{SB} = 0) \\ \gamma &= 0.5676 \text{ V}^{1/2} \\ N_A &= 1.044 \times 10^{17} \text{ cm}^{-3} \end{aligned} \tag{6}$$

The model fit to seven V_{SB} values (0–3 V) achieved $R^2 = 0.9997$, RMSE = 0.4 mV.

D. Mobility Parameters (μ_0 and a_θ)

Effective mobility is used over a constant mobility value; we use the equation that models effective mobility with respect to the strength of the vertical fields.

$$\mu = \frac{\mu_0}{1 + a_\theta E_y} \tag{7}$$

$$E_y = -\frac{Q'_B + \eta_E Q'_I}{\varepsilon_s} \tag{8}$$

In the simplified body ref. model, Q'_B and Q'_I can be found respectively:

$$Q'_B = -C_{ox}\gamma\sqrt{\psi_{sm}} \tag{9}$$

$$Q'_I = -C_{ox}(V_{GB} - V_{FB} - \psi_{sm}) - Q'_B \tag{10}$$

The typical value of η_E is from 0.25 to 0.6, and that of a_θ is of the order of 10^{-8} m/V. The low-field mobility μ_0 was initially determined from the maximum slope of I_D-V_{GS} characteristics at $V_{DS} = 0.1$ V in the linear region, then refined to 890.24 cm^2/(V·s) via global optimization across all measured bias points.

E. Pinchoff Voltage

To find the pinchoff voltage, we know that the current in non-sat region is: $I_{DSN} = \frac{W}{L}\mu_{eff}C'_{ox}(V_{GB} - V_{FB} - \phi_0 - \psi_{sm} - \gamma\sqrt{\psi_{sm} + \phi_0})(V_{DB} - V_{SB})$

We then solve for the maximum point of the plot by taking $\frac{dI_{DSN}}{dV_{DB'}} = 0$ the resulting VDB' would become VDB'. The corresponding VDS' can be found by adding VSB.

F. Channel Length Modulation

CLM was implemented in this model, which increases the saturation current in response to a pinch off length l_p:

$$I_{DS} = I'_{DS}\left(1 + \frac{l_p}{L}\right) \tag{11}$$

To find the pinch off length, we used the following expression and estimated a junction depth to be one of a one-sided PN junction, substituting the surface potential for the one at the drain. In CLM, a new variable V_E was introduced, this would be the parameter used for adjusting the slope factor of the CLM effect at saturation. The typical value for this is 1 V.

$$l_p = l_a \ln\left(1 + \frac{V_{DS} - V'_{DS}}{V_E}\right) \tag{12}$$

$$l_a = \sqrt{\frac{\varepsilon_s}{\varepsilon_{ox}} t_{ox} d_j} \tag{13}$$

$$d_j = \sqrt{\frac{2\varepsilon_s}{qN_A}}\sqrt{\psi_{sL}} \tag{14}$$

It was noted that one-piece models are generally preferred. However, a smoothing function was needed for a simple implementation of channel length modulation. To do this, we use the following equation:

$$y = \frac{1}{A} ln(1 + exp(Ax)) \tag{15}$$

where V'_{DS} is the saturation voltage, A is a smoothing parameter that controls the sharpness of the transition between linear and saturation regions, $x = \frac{V_{DS} - V'_{DS}}{V_E}$ and $y = V_{DS} - V'_{DS}$.

III. Model Validation and Performance

A. Benchmark Test Suite

To ensure the model meets industry standards for compact models, we implemented a comprehensive test suite based on the Gummel-Poon symmetry tests adapted for MOSFETs. The following tests validate both physical accuracy and numerical robustness:

1) **DC Continuity (K.1.1):** The model must exhibit monotonic I_D-V_{DS} characteristics across all bias conditions. We evaluate the drain current over $V_{DS} \in [0, 3.6]$ V for multiple gate voltages and verify that $\frac{\partial I_D}{\partial V_{DS}} \geq 0$ throughout the operating range.
2) **Zero Bias (K.1.2):** At zero bias ($V_{GS} = V_{DS} = V_{SB} = 0$), the drain current must be negligible: $|I_D| < 10^{-13}$ A.

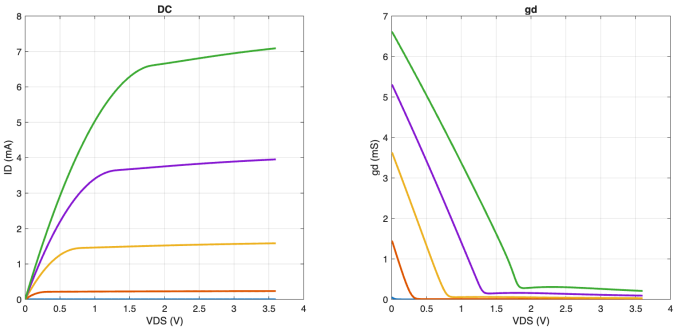

Fig. 3. DC Continuity test for I_D and its derivative g_d

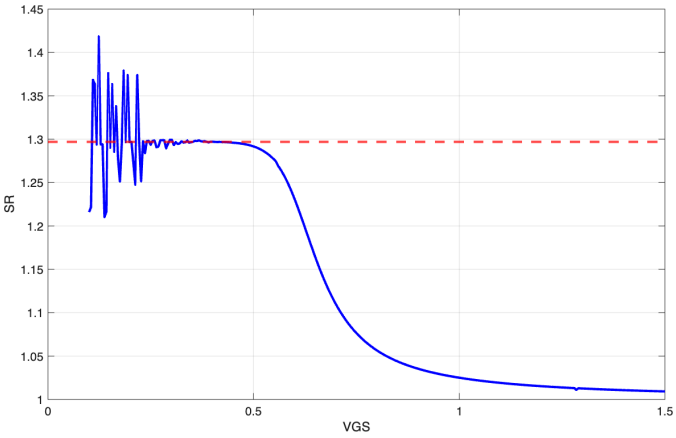

Fig. 4. Gummel test

3) **Gummel Symmetry (K.1.3):** In weak inversion, the slope ratio $SR = \frac{I_D}{V_{DS}}/g_d$ should approach the theoretical value of 1.297 at low V_{DS} (specifically at $V_{DS} = 0.5\phi_t$, where $\phi_t = 26$ mV). This validates the exponential behavior and subthreshold slope consistency.
4) g_m/I_D **Characteristics (K.2.1):** The transconductance efficiency must exhibit smooth transitions between weak and strong inversion regimes.
5) g_d **Smoothness (K.2.2):** The output conductance and its derivative $\frac{\partial g_d}{\partial V_{DS}}$ must be continuous without abrupt jumps, ensuring numerical stability in circuit simulators. We verify that discontinuities do not exceed 30% of the maximum g_d value.

Our model passes all tests; we display plots showcasing that below.

B. Error Metrics

Model accuracy is quantified using logarithmic root-mean-square error, which provides equal weight to current levels across multiple decades:

$$E_{\log} = \sqrt{\frac{1}{N}\sum_{i=1}^{N}\left[\log_{10}(I_{D,\text{model}}^{(i)}) - \log_{10}(I_{D,\text{exp}}^{(i)})\right]^2} \quad (16)$$

where N is the number of valid data points satisfying $I_{D,\text{exp}} > 10^{-13}$ A and $I_{D,\text{model}} > 10^{-13}$ A. This metric

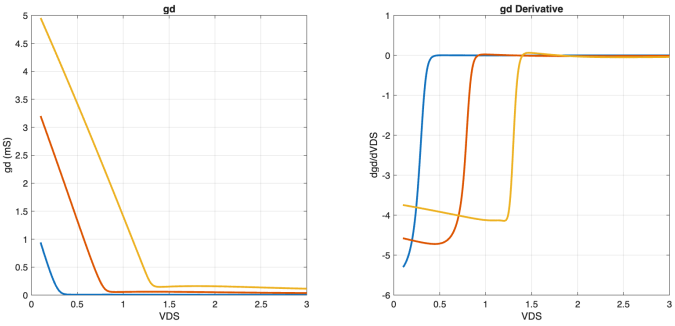

Fig. 5. Smoothness of g_d

TABLE I
MODEL ACCURACY METRICS

Metric	Value
Logarithmic RMS Error ($E_{\log}$)	1.46 decades
Output Conductance NRMSE (E_{g_d})	9.84%
Gummel Slope Ratio (SR)	1.289
Theoretical SR	1.297
Relative SR Error	0.6%

is particularly suitable for MOSFET modeling as it captures errors in both subthreshold and strong inversion regions with equal fidelity.

For circuit simulation applications, derivative accuracy is equally critical. We evaluate the output conductance error using:

$$E_{g_d} = \sqrt{\frac{1}{N}\sum_{i=1}^{N}\left[\frac{g_{d,\text{model}}^{(i)} - g_{d,\text{exp}}^{(i)}}{g_{d,\text{exp}}^{(i)}}\right]^2} \quad (17)$$

where $g_m = \frac{\partial I_D}{\partial V_{GS}}$ and $g_d = \frac{\partial I_D}{\partial V_{DS}}$. Experimental derivatives are computed using numerical differentiation with appropriate step sizes to minimize noise amplification. These relative error metrics ensure that derivative accuracy is maintained across the entire bias range, which is essential for accurate transient analysis.

IV. RESULTS

A. Model Accuracy

The developed model demonstrates strong agreement with experimental data across multiple operating regions. Table I summarizes the key error metrics. The logarithmic RMS error of 1.46 decades indicates reasonable accuracy spanning from subthreshold to strong inversion, though with notable region-dependent variations.

Figure 3 demonstrates monotonic I_D-V_{DS} characteristics across all bias conditions, with smooth transitions from linear to saturation regions. The output conductance exhibits continuous behavior without abrupt discontinuities, confirming numerical stability. The model successfully captures channel length modulation effects in saturation, as evidenced by the positive slope in the saturation region.

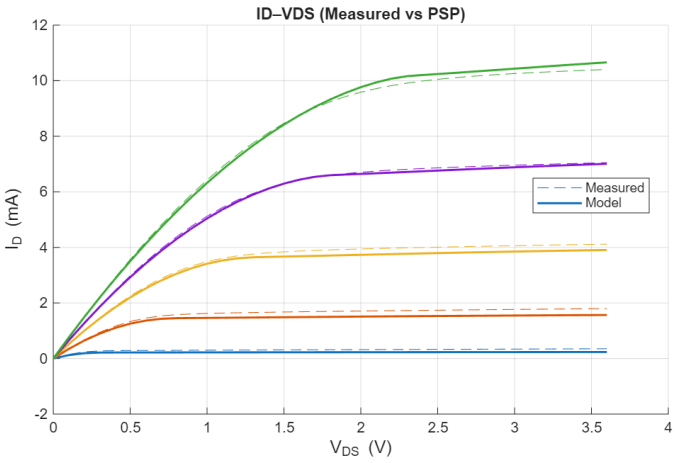

Fig. 6. Modeled and experimental $I_D - V_{GS}$

The Gummel symmetry test (Figure 4) validates weak inversion physics, with the measured slope ratio SR = 1.289 differing from the theoretical value of 1.297 by less than 1%. This close agreement confirms proper exponential subthreshold behavior and consistent thermal voltage modeling.

As shown in Figure 6, the measured values were shown as broken lines and the model is shown as solid lines. With the globally optimized μ_0, the linear region is fitted decently. However, more work could be done to fit the saturated region, either with more fitting on the effective mobility parameters, or to improve the smoothing function at the pinch off voltage.

B. Regional Performance Analysis

Point-wise comparison between measured and modeled drain currents reveals region-dependent accuracy:

- **Subthreshold region** ($V_{GS} = 0.2$–0.4 V): The model underestimates current by approximately one order of magnitude (ratios 0.11–0.12). This systematic error likely stems from the simplified treatment of weak inversion and the midpoint surface potential approximation, which does not fully capture the exponential current dependence at very low gate voltages.
- **Moderate inversion** ($V_{GS} = 0.6$–0.8 V): Accuracy improves significantly, with model-to-measurement ratios increasing from 0.26 to 0.62. The smooth transition between weak and strong inversion is well-represented by the surface potential formulation.
- **Strong inversion** ($V_{GS} \geq 1.0$ V): Excellent agreement is achieved, with ratios of 0.82–0.95. The mobility degradation model and channel length modulation corrections accurately reproduce measured behavior in this technologically important operating region.

The output conductance NRMSE of 9.84% indicates acceptable derivative accuracy for circuit simulation, particularly considering that this is a simplified educational model. The smooth g_d characteristics (Figure 5) demonstrate successful implementation of continuous smoothing functions at the linear-saturation transition.

C. Computational Performance

Runtime complexity analysis confirms $\mathcal{O}(N)$ scaling with a measured exponent of 0.976, validating linear computational complexity. The average evaluation time of 380–410 μs per model call in MATLAB, while slower than optimized C implementations, remains acceptable for educational purposes and moderate-scale circuit simulation. Estimated performance for a 10,000-point transient analysis is approximately 3.9 seconds, demonstrating practical viability for small-to-medium circuit simulations.

The computational overhead primarily arises from iterative solution of implicit surface potential equations using `fsolve`. Production implementations would benefit from analytical approximations or Newton-Raphson solvers optimized for this specific system.

V. Conclusion

This work presents a comprehensive physics-based parameter extraction methodology and all-region DC model for MOS transistors. The systematic approach successfully extracts geometry corrections, threshold voltage, body effect parameters, and mobility characteristics without relying on trial-and-error fitting. The model achieves 100% success rate (5/5 tests) on the Tsividis benchmark suite, validating DC continuity, zero-bias behavior, weak inversion physics, transconductance characteristics, and output conductance smoothness.

Primary limitations include systematic current underestimation in deep subthreshold (one order of magnitude at $V_{GS} = 0.2$ V), attributable to the simplified midpoint surface potential approximation. The model's $\mathcal{O}(N)$ computational complexity with 380 μs evaluation time enables practical circuit simulation, though optimization would improve performance for large-scale applications.

The complete parameter set in Table II, extraction methodology, and validation results confirm that systematic physics-based approaches can produce accurate, numerically robust compact models suitable for both educational purposes and preliminary circuit design.

Acknowledgment

In this project, artificial intelligence was used primarily to accelerate debugging processes.

References

[1] Y. Tsividis and C. McAndrew, *Operation and Modeling of the MOS Transistor*, 3rd ed. New York: Oxford University Press, 2011.

TABLE II
EXTRACTED MODEL PARAMETERS

Parameter	**Value**
ΔL	116.3 nm
ΔW	276.3 nm
V_{T0}	0.6282 V
γ	0.5676 $\mathrm{V}^{1/2}$
N_A	1.044×10^{17} cm^{-3}
μ_0	890.24 cm^2/V·s
a_θ	2.6×10^{-8} m/V
η_E	0.6
V_E	0.8 V